JJMS **19**, No. 2, 351-367 (2026)


Jordan Journal of Mathematics and Statistics.
*Yarmouk University*

DOI:https://doi.org/10.47013/19.2.15

# Finite element analysis for strongly damped wave equation

*Mohammed Homod Hashim*[1], *Sattar M. Hassan*[2], *Akil J. Harfash*[3,*]

[1] Department of Mathematics, College of Sciences, University of Basrah, Basrah, Iraq
[2] Department of Mathematics, College of Education, University of Misan, Misan, Iraq
[3] Department of Mathematics, College of Sciences, University of Basrah, Basrah, Iraq

Received: Jan. 30, 2025 Accepted : Oct. 26, 2025

**Abstract:** Finite element methods (FEMs) for the strongly damped wave equation with semi- and fully discrete solutions are presented in this paper. First, a system of first-order equations with respect to time was created from the strongly damped wave equation. We established the solution spaces for the numerical solution by identifying the stability bounds of the solution. Convergence to the continuous solution is demonstrated as part of the analysis. Additionally, a practicable algorithm is suggested to effectively solve the fully-discrete formulation at each time step. The calculations are performed in one, two, and three spatial dimensions, demonstrating the efficacy of the suggested methodology. The special characteristics of the study include the thorough transformation of the second-order equation into a first-order system in time, the establishment of weak solutions, the proof and derivation of stability bounds, and a convergence analysis of the proposed FEM schemes.

**Keywords:** damped wave equation; semi-discrete; fully-discrete; stability bounds; existence.

**2010 Mathematics Subject Classification**. 65M60; 65M12; 35D30.

## 1 Introduction

Since it accurately simulates situations involving both wave propagation and damping phenomena, the strongly damped wave equation is essential in many fields. This equation is widely used in tsunami analysis, where it is used to simulate wave dynamics in the wave equation form of the continuity equation [31]. In structural mechanics, this equation is also crucial for the study of dynamic boundary conditions and viscoelastic materials. It facilitates the study of attractors and the comprehension of these systems' long-term behavior [16]. The strongly damped wave equation is a key tool in mathematical physics for stability analysis and developing control plans for dynamic systems. For instance, exact controllability issues are addressed using spectral decomposition techniques, which offer important insights into system behavior [47]. In order to predict and control system behavior in engineering contexts, the strongly damped wave equation is also used to solve inverse problems and identify parameters [13]. The equation is an effective tool for studying partial differential equations and numerical simulations because of the strong damping term, which is crucial for regularizing and stabilizing solutions [14].

In this article, our focus is on the numerical solution of the following strongly damped nonlinear wave equation [44]: ($\varPhi$) Find $\{s\}$ such that

$$s_{tt} + s_t - \Delta s_t - \Delta s + s^3 = 0 \qquad \text{in} \quad \varPsi \times (0, \mathscr{M}), \tag{1}$$

$$\frac{\partial s}{\partial \nu} = 0 \qquad \text{on} \quad \partial\varPsi \times (0, \mathscr{M}), \tag{2}$$

$$s(\mathbf{x}, 0) = s_1^0(\mathbf{x}), \quad s_t(\mathbf{x}, 0) = s_2^0(\mathbf{x}), \quad \text{in} \quad \varPsi. \tag{3}$$

* Corresponding author e-mail: akil.harfash@uobasrah.edu.iq

where $\Psi$ is an open bounded domain in $\mathbb{R}^d$, $d \geq 1$ with a smooth boundary $\partial\Psi$, $s$ is the displacement of the wave field, $\nu$ represents the outward unit normal to $\partial\Psi$, and $s_1^0(\mathbf{x})$ and $s_2^0(\mathbf{x})$ are both given real smooth functions.

Problems (1)-(3) describe a wide range of physical phenomena, such as the longitudinal and transversal vibrations of string and bar, respectively, with viscous effects [15], and the variation of a homogeneous and isotropic viscoelastic material [44]. In quantum physics, equation (1) also appears as a Klein-Gordon equation for perturbed waves [44]. The results of regularity and the globally existing strong solution have been shown in [53] and the cited works. [41,42] offers more numerical techniques for solving the high-dimensional sinh-Gordon equation and the modified Klein-Gordon-Zakharov equations. For numerical approximations and without the strong operator $-\Delta s_t$, a three-level compact finite difference scheme and a nonlinear difference scheme have been presented in [39,38,1,32].

The damped wave equation has applications in fields such as seismic research, electromagnetics, and acoustics, making its numerical solution crucial. The damped wave equation, which is a partial differential equation, illustrates the necessity for accurate numerical methods by representing a variety of physical processes involving wave propagation with damping effects. To solve the strongly damped wave equation, FEMs have been used extensively. Significant advancements in the numerical treatment of these complex equations have been demonstrated, highlighting their application in viscoelastic theory and other internally damped systems [33]. Maximum-norm estimates for finite-element methods have received attention, offering strong mathematical foundations to improve and comprehend the damped wave equation's numerical approximations [51]. A nonstandard finite difference scheme for the damped wave equation was presented in [36], guaranteeing the maintenance of positivity in numerical simulations. This method shows promise for faithfully capturing wave behaviors when damping is present.

As demonstrated in [17], high-order explicit local time-stepping techniques have been introduced to effectively address damped wave equations. These techniques are particularly helpful for simulations that require a high degree of computational efficiency and precision. In [46], the locally damped wave equation was studied, with an emphasis on the creation of FEMs for hyperbolic equations. The study provided insightful information about the numerical difficulties and solutions associated with controlling local damping effects in wave propagation. Real-world wave phenomena must be accurately simulated, and recent advances in nonlinear strongly damped wave equations have shown that numerical methods can achieve second-order accuracy in both space and time [30].

Prior research on FEM for damped wave equations frequently concentrated on linear models or semi-discrete formulations, where the damping term manifests as a lower-order contribution. For instance, [43] established error estimates mainly in one-dimensional settings by analyzing a Galerkin FEM for the strongly damped linear wave equation. The nonlinear cubic term and the diffusive damping term $-\Delta s_t$, which both have a substantial impact on solution regularity and stability, are not addressed by these formulations, which typically assume smooth data and linear damping. Although later works, like [48], expanded the semi-discrete analysis to include non-smooth initial data, they only addressed linearized problems and did not offer convergence proofs for fully discrete schemes. In addition, the combined effects of strong damping and nonlinearity in multi-dimensional domains, where it is more difficult to establish the stability and convergence behavior of the discretized system, are not typically explored in numerical studies. While recent studies such as [34] have examined generalized FEMs for strongly damped wave equations with heterogeneous coefficients, they mainly concentrated on linear models and spatial multiscale analysis, largely ignoring the time discretization and nonlinear damping aspects.

This paper aims to rectify these gaps by constructing a full theoretical and numerical theory for semi-discrete and fully discrete finite element methods applied to the nonlinear strongly damped wave equation. The paper is devoted for establishing the existence and stability of the discrete solution, deriving a priori estimates, verifying the convergence towards the continuous solution. In addition, one derives a machine- amenable algorithm for solving this fully discrete nonlinear system at each time step, which renders the method computationally feasible in higher dimensions. Extensive numerical experiments in one, two and three spatial dimensions are carried out to validate the proposed method, which indicate uniform error reduction and stability as well as the ability of handling smooth and non-smooth initial data. Therefore, the present work closes a theoretical and computational gap by proposing an unified and stable FEM framework for strongly damped nonlinear wave problems in multiple dimensions.

To numerically approximate Eqs.(1)-(3), the strongly damped wave equation was first recast in a first-order time-dependent system formulation by adding an artificial variable $q = s_t + s$. The resulting coupled system was subsequently discretized in space by the standard Galerkin finite element scheme with continuous piecewise linear functions as basis. The weak form was obtained by multiplying both sides of each equation by a test function and integrating over the spatial domain, with Neumann boundary conditions as defined in Eq. (2). The spatially discrete system was evolved in time using an implicit backward Euler scheme. This method guarantees unconditional stability for the strongly damped dynamics. Combining spatial and temporal discretization results in a stable and convergent fully discrete formulation. This makes it easy to replicate the results in any standard FEM environment. Because numerical solutions to differential equations are crucial, many recent studies have focused on solving various equations using different numerical methods [24,29,2,52].

In this study, we consider $q = s_t + s$, which allows System (1)-(3) to be reformulated as follows:

$$\partial_t q - \Delta q + s^3 = 0, \tag{4}$$

$$\partial_t s + s - q = 0, \tag{5}$$

$$\frac{\partial s}{\partial \nu} = 0 \qquad \text{on} \quad \partial\Psi \times (0, \mathscr{M}), \tag{6}$$

$$s(\mathbf{x}, 0) = s_1^0(\mathbf{x}), \quad q(\mathbf{x}, 0) = s_1^0(\mathbf{x}) + s_2^0(\mathbf{x}) = q^0(\mathbf{x}) \qquad \text{in} \quad \Psi. \tag{7}$$

Subsequently, we present a weak formulation of System (4) and (5) expressed as follows:

($\Phi$) Find $s(\mathbf{x},t), q(\mathbf{x},t) \in H^1(\Psi)$ such that $s(\mathbf{x},0) = s_1^0(\mathbf{x})$ and $q(\mathbf{x},0) = q^0(\mathbf{x})$ and for almost every $t \in (0, \mathscr{M})$, we have that

$$(\partial_t q, \eta) + (\nabla q, \nabla \eta) + (s^3, \eta) = 0, \qquad \forall \ \eta \in H^1(\Psi), \tag{8}$$

$$(\partial_t s, \eta) + (s, \eta) - (q, \eta) = 0, \qquad \forall \ \eta \in H^1(\Psi). \tag{9}$$

The current study adds to the numerical analysis of the strongly damped nonlinear wave equation. It presents a clear framework that combines semi-discrete and fully discrete finite element methods. Unlike typical weakly damped or linear models, adding a strong damping term (related to the Laplacian of the velocity) creates more mathematical complexity and stiffness. This requires special numerical methods to ensure stability and accuracy. The papers originality lies in the careful transformation of the second-order equation into a first-order system over time. It also includes the derivation and proof of stability bounds, the existence of weak solutions, and the convergence analysis of the proposed FEM methods. In addition, an efficient algorithm is developed to solve the fully discrete nonlinear system at each time step, connecting theoretical analysis with practical use.

The notations utilized in this paper are outlined in Section 2. In Section 3, we present the standard piecewise linear FEM to derive a semi-discrete approximation and detail the necessary assumptions regarding the partitioning of $\Psi$. Section 4 formulates the semi-discrete approximation of problem ($\Phi$) and establishes its existence. Section 5 introduces a fully practical FEM of ($\Phi$), along with stability estimates for the fully-discrete approximations. In Sections 5.1 and 5.2, we demonstrate the existence of a fully-discrete approximation and a weak solution, respectively. In Section 6, we conduct the computations in one, two, and three dimensions to validate the theoretical findings presented earlier. All simulations were executed using programs developed in Matlab. Section 6.1 outlines a practical algorithm for computing the approximated solution. In Section 6.2, we analyze the computational error associated with the fully-discrete error bound across one, two, and three dimensions. Additionally, Section 6.3 provides simulation results specifically for two-dimensional cases.

## 2 Notation and Preliminaries

The space $L^2(\Psi)$, defined over $\Psi$ and associated with the norm $\|\cdot\|_0$, is equipped with an inner product denoted by $(\cdot,\cdot)$. Additionally, the notation $\langle\cdot,\cdot\rangle$ signifies the duality pairing between the dual space $(H^1(\Psi))'$ and $H^1(\Psi)$, where $(H^1(\Psi))'$ is the dual of $H^1(\Psi)$. A norm for the dual space $(H^1(\Psi))'$ is defined as follows:

$$\|\gamma\|_{(H^1(\Psi))'} := \sup_{\eta \neq 0} \frac{|\langle \gamma, \eta \rangle|}{\|\eta\|_1} \equiv \sup_{\|\eta\|_1 = 1} |\langle \gamma, \eta \rangle|. \tag{10}$$

Additionally, we define the function spaces that depend on both time and space as $L^\alpha(0, \mathscr{M}; \Gamma)$ where $1 \leq \alpha \leq \infty$, and $\Gamma$ represents a Banach space. These spaces include all functions $\gamma$ such that for almost every $s \in (0, \mathscr{M})$, $\gamma \in \Gamma$, and the following norm remains finite [35]:

$$\|\gamma(s)\|_{L^\alpha(0,\mathscr{M};\Gamma)} = \left( \int_0^{\mathscr{M}} \|\gamma(s)\|_\Gamma^\alpha ds \right)^{\frac{1}{\alpha}},$$

$$\|\gamma(s)\|_{L^\infty(0,\mathscr{M};\Gamma)} = ess \sup_{s \in (0,\mathscr{M})} \|\gamma(s)\|_\Gamma.$$

Additionally, we define the spaces $L^\alpha(\Psi_{\mathscr{M}}) = L^\alpha(0, \mathscr{M}; L^\alpha(\Psi))$, $\alpha \in [1, \infty]$. Also, we define $C([0, \mathscr{M}]; \Gamma)$, the space of continuous functions from $[0, \mathscr{M}]$ into $\Gamma$, which consists of $\gamma(s) : [0, \mathscr{M}] \to \Gamma$ so that $\gamma(s) \to \gamma(s_0)$ in $\Gamma$ as $s \to s_0$. The norm which is associated to the space $C([0, \mathscr{M}]; \Gamma)$ can be defined as [49]:

$$\|\gamma(s)\|_{C([0,\mathscr{M}];\Gamma)} = \sup_{s \in [0,\mathscr{M}]} \|\gamma(s)\|_\Gamma.$$

Additionally, we need the following outcomes as presented in [9,10]:

$$H^1(\Psi) \overset{c}{\hookrightarrow} L^\rho(\Psi) \hookrightarrow (H^1(\Psi))' \text{ holds for } \rho \in \begin{cases} [1,\infty] & \text{if } d=1, \\ [1,\infty) & \text{if } d=2, \\ [1,6] & \text{if } d=3. \end{cases} \tag{11}$$

## 3 FE spaces and associated results

FEM is used in this study because it offers a flexible and mathematically sound approach for approximating the strongly damped nonlinear wave equation. This equation includes second-order spatial derivatives and a diffusive damping term, $-\Delta s_t$. Such equations often appear in complex geometries, varied materials, and nonlinear dynamic systems, where analytical solutions are usually not available. Finite difference methods may also face problems with stability and boundary conditions. FEM easily handles irregular shapes and Neumann or mixed boundary conditions. This allows for precise spatial discretization without losing geometric flexibility. Additionally, its variational formulation helps ensure that the discrete problem keeps important properties of the continuous system, such as energy stability and conservation laws, which are crucial for managing strongly damped dynamics. The method also allows for careful control over approximation accuracy by refining the mesh and choosing basis functions. This makes calculations efficient in one-, two-, and three-dimensional contexts. Therefore, FEM combines strong theoretical foundations with efficient computation, making it especially well-suited for the stable and convergent numerical solution of the strongly damped wave equation.

Let $\Upsilon \subset H^1(\Psi)$ represent a FE space defined by:

$$\Upsilon = \{\omega \in C(\overline{\Psi}) : \omega|_\tau \text{ is linear } \forall \tau \in \mathscr{T}\}.$$

Let $\{x_i\}_{i=1}^J$ denote the set of nodes of $\tau$, and let $\{\eta_i\}_{i=1}^J$ represent a basis for $\Upsilon$ defined by $\eta_i(x_j) = \delta_{ij}$, for $i,j = 0,\dots,J$. Let $\pi : C(\overline{\Psi}) \to \Upsilon$ be the Lagrange interpolation operator such that $\pi\omega(x_i) = \omega(x_i)$, for $i = 0,\dots,J$. Additionally, define a discrete $L^2$ inner product on $C(\overline{\Psi})$ as follows:

$$(\omega_1,\omega_2) = \int_\Psi \pi\{\omega_1(x)\omega_2(x)\}d\mathbf{x} \equiv \sum_{i=0}^{J} \widehat{M}_{ii}\omega_1(x_i)\omega_2(x_i), \tag{12}$$

where $m_i = (\varphi(\eta_i),\varphi(\eta_i)) = (1,\varphi(\eta_i)) > 0$ which is called the lumped mass matrix. We can show that

$$(\pi\omega_1,\omega_2) := (\omega_1,\omega_2) \quad \forall \omega_1,\omega_2 \in C(\overline{\Psi}). \tag{13}$$

If $\kappa_{ij} := (\nabla\varphi_i,\nabla\varphi_j)$, then as the partitioning $\mathscr{T}$ is acute, we have that (see [40] page 49)

$$\kappa_{jj} > 0, \forall j \;\text{ and }\; \kappa_{ij} \leq 0, \forall i \neq j. \tag{14}$$

We define $\kappa_{ij} := (\nabla\varphi_i,\nabla\varphi_j)$, where $\varphi_i$ and $\varphi_j$ are basis functions. The induced norm $\|\cdot\|_= [(\cdot,\cdot)]^{\frac{1}{2}}$ on the finite-dimensional space $\Upsilon$ is equivalent to the standard $L^2$-norm $\|\cdot\|_0 = [(\cdot,\cdot)]^{\frac{1}{2}}$. The following essential properties of the space $\Upsilon$ are established and can be found in detail in [45,12]:

$$C_1\|\vartheta\|_0 \leq |\vartheta| \leq C_2\|\vartheta\|_0, \quad \forall \vartheta \in \Upsilon. \tag{15}$$

For every $\delta(x) \in \Upsilon$, we define the following:

$$|\delta|_{,r} := \Big(\int_\Psi \pi\{|\delta(x)|^r\}d\mathbf{x}\Big)^{\frac{1}{r}} \equiv \Big(\sum_{i=0}^{k} \widehat{M}_{jj}|\delta(x_i)|^r\Big)^{\frac{1}{r}} \text{ if } 0 \leq r < \infty, \tag{16}$$

and

$$|\delta|_{,\infty} := \max_{0\leq j\leq k} |\delta(x_j)|, \qquad \text{if } r = \infty. \tag{17}$$

The discrete Minkowski and Hölder inequalities can be defined for all $\delta_1,\delta_2 \in C(\overline{\Psi})$ (and thus also for elements in $\Upsilon$), as outlined in [37] on pages 271-274, as follows:

$$|(\delta_1,\delta_2)| \leq |\delta_1|_{,r_1}|\delta_2|_{,r_2}, \quad \frac{1}{r_1}+\frac{1}{r_2} = 1, \quad 0 \leq r_1,r_2 \leq \infty, \tag{18}$$

$$\left|\delta_1+\delta_2\right|_{,r} \le |\delta_1|_{,r}+|\delta_2|_{,r}, \quad 0\le r\le\infty. \tag{19}$$

We require the following estimate, as stated in [50]:

$$|\left(\delta_1,\delta_2\right)-\left(\delta_1,\delta_2\right)| \le Ch^{k+1}\|\delta_1\|_k\|\delta_2\|_1, \text{ for all } \delta_1,\delta_2\in\Upsilon \;, k=0 \text{ or } 1. \tag{20}$$

We also require the following properties, as stated in [11]:

$$\|(I-\pi)\delta\|_0+h|(I-\pi)\delta|_1 \le Ch^2|\delta|_2, \text{ for all } \delta\in H^2(\Psi), \tag{21}$$

$$\|(I-\pi)\delta\|_{0,1} \le Ch^2|\delta|_{2,1}, \text{ for all } \delta\in\widetilde{\mathbb{W}}^{2,1}(\Psi)\ d\le 3. \tag{22}$$

It is also helpful to present the following result: For $1\le r<\infty$, we have the relation:

$$|\delta|_{2,r} \le \left(\int_\Psi\sum_{k,n}^{k}\left|\frac{\partial^2\delta}{\partial x_k x_\ell}\right|^r d\mathbf{x}\right)^{\frac{1}{r}} \le 2^{\frac{1}{r}}|\delta|_{2,r}, \text{ for all } \delta\in\widetilde{\mathbb{W}}^{2,r}(\Psi). \tag{23}$$

The inverse inequalities are also presented here: For every $\delta\in\Upsilon$, as shown in [10], the following holds:

$$|\delta|_{1,r,"\tau"} \le Ch^{-1}_{,"\tau"}|\delta|_{0,r,"\tau"}, \quad 1\le r\le\infty, \tag{24}$$

$$\|\delta\|_{0,r_2,"\tau"} \le Ch_{,"\tau"}^{-d(\frac{1}{r_1}-\frac{1}{r_2})}\|\delta\|_{0,r_1,"\tau"}, \quad 1\le r_1\le r_2\le\infty, \tag{25}$$

$$|\delta|_{1,r_2,"\tau"} \le Ch_{,"\tau"}^{-d(\frac{1}{r_1}-\frac{1}{r_2})}|\delta|_{1,r_1,"\tau"}, \quad 1\le r_1\le r_2\le\infty, \tag{26}$$

where the abbreviation "$\tau$" means "with" or "without" $\tau$.

We require the following interpolation results: For every $\eta\in\widetilde{\mathbb{W}}^{1,m_2}(\Omega)$, where $m_2\in[2,\infty]$ if $d=1$ and $m_2\in(d,\infty]$ if $d=2$ or 3, the following holds:

$$|(I-\pi)\eta|_{m_1,m_2} \le Ch^{1-m_1}|\eta|_{1,m_2}, \quad m_1\in\{0,1\}, \tag{27}$$

$$\lim_{\to 0}\|(I-\pi)\eta\|_{1,m_2}=0. \tag{28}$$

The following inequalities is required [8]:

$$C_1h^2|\eta|_1 \le C_2h\|\eta\|_0 \le \|\eta\|_{-h} \le \|\eta\|_{-1} \le C_3\|\eta\|_{-h}, \ \forall\eta\in\Upsilon. \tag{29}$$

Let $P: L^2\to\Upsilon$ be the orthogonal projection from $L^2$ onto $\Upsilon$, then it satisfies:

$$(P\rho,\vartheta^k)=(\rho,\vartheta^k), \quad \text{for all } \ \rho\in L^2,\ \vartheta^k\in\Upsilon. \tag{30}$$

We require the following projection property:

$$\|P\vartheta\|_1 \le C\|\vartheta\|_1, \quad \text{for all } \ \vartheta\in H^1. \tag{31}$$

## 4 A semi-discrete approximation

We introduce the subsequent semi-discrete approximation of the system (4)-(7):
($\Phi$) Find $\{s,q\}\in\Upsilon\times\Upsilon$ such that for $a.e.\ t\in(0,\mathscr{M})$

$$(\partial_t q,\eta)+(\nabla q,\nabla\eta)+((s)^3,\eta)=0, \qquad \forall\eta\in\Upsilon, \tag{32}$$

$$(\partial_t s,\eta)+(s,\eta)-(q,\eta)=0, \qquad \forall\eta\in\Upsilon, \tag{33}$$

$$s(x,0)=Ps_1^0(x), \quad q(x,0)=Ps_1^0(x)+Ps_2^0(x)=Pq^0(x). \tag{34}$$

### 4.1 Global existence

**Theorem 1.** *Assume that $\Psi\subset\mathbb{R}^d$ $(d\le 3)$ is an open, bounded, and convex domain. Let $s^0,q^0\in H^1(\Psi)$. Then, the system (32)-(34) admits a solution $\{s q\}$, which satisfies the following conditions:*

$$s\in L^\infty(0,\mathscr{M};L^4(\Psi)), \tag{35}$$

$$q\in L^\infty(0,\mathscr{M};L^4(\Psi))\cap L^2(0,\mathscr{M};H^1(\Psi)), \tag{36}$$

$$\partial_t s\in L^2(0,\mathscr{M};(L^2(\Psi))'), \tag{37}$$

$$\partial_t q\in L^{\frac{3}{4}}(0,\mathscr{M};(H^1(\Psi))'). \tag{38}$$

**Proof**: We select $\eta = q$ in (32) and $\eta = \pi(s)^3$ in (33) to obtain the result that

$$(\partial_t q, q) + (\nabla q, \nabla q) + ((s)^3, q) = 0, \tag{39}$$

$$(\partial_t s, \pi(s)^3) + (s, \pi(s)^3) - (q, \pi(s)^3) = 0. \tag{40}$$

By merging (39) and (40), we arrive at the following result

$$\frac{d}{2dt}\int_\Psi \pi|q|^2dx + \frac{d}{4dt}\int_\Psi \pi|s|^4dx + \int_\Psi \pi|s|^4dx + \int_\Psi \pi|\nabla q|^2dx = 0. \tag{41}$$

By performing an integration of both sides of equation (41) over the time interval $(0,\mathscr{M})$, we arrive at the result that

$$\frac{1}{2}|q(\mathscr{M})|^2 + \frac{1}{4}\|s(\mathscr{M})\|_{0,4}^4 + \int_0^{\mathscr{M}} |s|_{,4}^4dt + \int_0^{\mathscr{M}} |q|_1^2dt \le C\mathscr{M}|\Psi|. \tag{42}$$

From (42) and (15), we have that

$$\|q\|_{L^\infty(0,\mathscr{M};L^2(\Psi))} \le C, \quad \|s\|_{L^\infty(0,\mathscr{M};L^4(\Psi))} \le C, \quad \|s\|_{L^4(\Psi_{\mathscr{M}})} \le C, \quad \|q\|_{L^2(0,\mathscr{M};H^1(\Psi))} \le C. \tag{43}$$

By integrating (32) over $(0,t)$ and applying Hölder's inequality, it follows, for all $\eta \in L^4(0,\mathscr{M};H^1(\Psi))$, that

$$\left|\int_0^{\mathscr{M}}\int_\Psi \partial_t q^\eta\, dxdt\right|$$

$$\le \left[\|q^\|_{L^2(0,\mathscr{M};H^1(\Psi))}\|\eta^\|_{L^2(0,\mathscr{M};H^1(\Psi))} + \|s^\|_{L^4(\Psi_{\mathscr{M}})}^3\|\eta^\|_{L^4(\Psi_{\mathscr{M}})}\right] \tag{44}$$

Utilizing equation (43) and recognizing the embeddings $L^4(0,\mathscr{M};H^1(\Psi)) \hookrightarrow L^2(0,\mathscr{M};H^1(\Psi))$ and $L^4(0,\mathscr{M};H^1(\Psi)) \hookrightarrow L^4(\Psi_{\mathscr{M}})$, we conclude that

$$\left|\int_0^{\mathscr{M}}\int_\Psi \partial_t q^\eta\, dxdt\right| \le C\|\eta\|_{L^4(0,\mathscr{M};H^1(\Psi))}.$$

This will produce the ensuing outcome:

$$\|\partial_t q\|_{L^{\frac{3}{4}}(0,\mathscr{M};(H^1(\Psi))')} = \sup_{\eta\neq 0}\frac{|\int_0^{\mathscr{M}}\int_\Psi \partial_t q\eta\, dxdt|}{\|\eta\|_{L^4(0,\mathscr{M};H^1(\Psi))}} \le C,$$

which means that

$$\partial_t q \in L^{\frac{3}{4}}(0,\mathscr{M};(H^1(\Psi))'). \tag{45}$$

By performing the integration of (33) over the interval $(0,\mathscr{M})$ and applying Hölder's inequality, it can be deduced that, for every $\eta \in L^2(\Psi_{\mathscr{M}})$, the following holds:

$$\left|\int_0^{\mathscr{M}}\int_\Psi \partial_t s^\eta\, dxdt\right|$$

$$\le \left[\|s^\|_{L^2(\Psi_{\mathscr{M}})}\|\eta^\|_{L^2(\Psi_{\mathscr{M}})} + \|q^\|_{L^2(\Psi_{\mathscr{M}})}\|\eta^\|_{L^2(\Psi_{\mathscr{M}})}\right]. \tag{46}$$

Subsequently, by employing (43), it follows that:

$$\left|\int_0^{\mathscr{M}}\int_\Psi \partial_t q^\eta\, dxdt\right| \le C\|\eta\|_{L^2(\Psi_{\mathscr{M}})}.$$

This will lead to the following result

$$\|\partial_t s\|_{L^2(0,\mathscr{M};(L^2(\Psi))')} = \sup_{\eta\neq 0}\frac{|\int_0^{\mathscr{M}}\int_\Psi \partial_t s\eta\, dxdt|}{\|\eta\|_{L^2(\Psi_{\mathscr{M}})}} \le C,$$

which give the following result

$$\partial_t s \in L^2(0,\mathscr{M};(L^2(\Psi))'). \tag{47}$$

## 5 A fully-discrete approximation

Let $\mathscr{L}$ be a positive integer, and define the time step as $\delta t := \frac{\mathscr{M}}{\mathscr{L}}$. We now consider the following fully-discrete FE approximation of the system (4)-(7):
$(\Phi^{,\delta t})$ Find $S^\ell(.,t), Q^\ell(.,t) \in \Upsilon \times \Upsilon$ such that $\forall \eta \in \Upsilon$

$$\left(\frac{Q^\ell - Q^{\ell-1}}{\delta t}, \eta\right) + (\nabla Q^\ell, \nabla \eta) + ((S^\ell)^3, \eta) = 0, \ \forall \eta \in \Upsilon, \tag{48}$$

$$\left(\frac{S^\ell - S^{\ell-1}}{\delta t}, \eta\right) + (S^\ell, \eta) - (Q^\ell, \eta) = 0, \ \forall \eta \in \Upsilon, \tag{49}$$

$$S^0 = Ps^0, \quad Q^0 = Pq^0. \tag{50}$$

For future reference, it is important to record the following facts:

$$2\kappa(\kappa - \lambda) = \kappa^2 + (\kappa - \lambda)^2 - \lambda^2, \ \forall \kappa, \lambda \in \mathbb{R}. \tag{51}$$

**Theorem 2.** *Let $s_0, q_0 \in H^1(\Psi) \cap L^4(\Psi)$. Then, for any $\delta t > 0$, there exists a solution $\{S^\ell, Q^\ell\}_{\ell=1}^{\mathscr{L}}$ to $(\Phi^{,\delta t})$. The following stability bounds are then valid:*

$$\max_{m=1,..,\mathscr{L}} \left[\|Q^m\|^2 + \|S^m\|_{0,4}^4 + \|S^m\|^2\right] + \sum_{\ell=1}^m \|Q^\ell - Q^{\ell-1}\|^2 + \sum_{\ell=1}^m \|S^\ell - S^{\ell-1}\|^2$$
$$+2\sum_{\ell=1}^m \delta t \|\nabla Q^\ell\|_0^2 + \sum_{\ell=1}^m \delta t \|S^\ell\|_{0,4}^4 + 2\sum_{\ell=1}^m \delta t \|S^\ell\|_0^2 \le C(\delta t)^3. \tag{52}$$

**Proof**: By selecting $\eta = Q^\ell$ in (48), and $\eta = \pi(S^\ell)^3$ and $\eta = S^\ell$ in (49), we obtain the following results:

$$\frac{1}{\delta t}(Q^\ell - Q^{\ell-1}, Q^\ell) + (\nabla Q^\ell, \nabla Q^\ell) + ((S^\ell)^3, Q^\ell) = 0, \tag{53}$$

$$\frac{1}{\delta t}(S^\ell - S^{\ell-1}, \pi(S^\ell)^3) + (S^\ell, \pi(S^\ell)^3) - (Q^\ell, \pi(S^\ell)^3) = 0, \tag{54}$$

$$\frac{1}{\delta t}(S^\ell - S^{\ell-1}, S^\ell) + (S^\ell, S^\ell) - (Q^\ell, S^\ell) = 0. \tag{55}$$

From (53), (54), and (55), it follows that

$$\frac{1}{\delta t}(Q^\ell - Q^{\ell-1}, Q^\ell) + \frac{1}{\delta t}(S^\ell - S^{\ell-1}, \pi(S^\ell)^3) + \frac{1}{\delta t}(S^\ell - S^{\ell-1}, S^\ell)$$
$$+(\nabla Q^\ell, \nabla Q^\ell) + (S^\ell, \pi(S^\ell)^3) + (S^\ell, S^\ell) = (Q^\ell, S^\ell). \tag{56}$$

Taking into account (51), Hölder's and Young's inequalities, as well as (15) and (5), we deduce that:

$$\frac{1}{2\delta t}\|Q^\ell\|^2 + \frac{1}{2\delta t}\|Q^\ell - Q^{\ell-1}\|^2 + \frac{1}{2\delta t}\|S^\ell\|^2 + \frac{1}{2\delta t}\|S^\ell - S^{\ell-1}\|^2 + \frac{1}{2\delta t}\|S^\ell\|_{,4}^4 + \|\nabla Q^\ell\|_0^2 + \|S^\ell\|_{,4}^4$$
$$+\|S^\ell\|^2 \le \frac{1}{2\delta t}\|Q^{\ell-1}\|^2 + \frac{1}{2\delta t}\|S^{\ell-1}\|^2 + \frac{1}{2\delta t}\|S^{\ell-1}\|_{,4}^4 + \frac{1}{4\delta t}\|Q^\ell\|^2 + \delta t\|S^\ell\|^2$$
$$\le \frac{1}{2\delta t}\|Q^{\ell-1}\|^2 + \frac{1}{2\delta t}\|S^{\ell-1}\|^2 + \frac{1}{2\delta t}\|S^{\ell-1}\|_{,4}^4 + \frac{1}{4\delta t}\|Q^\ell\|^2 + \frac{1}{2}\|S^\ell\|_{,4}^4 + C(\delta t)^2. \tag{57}$$

Adding the given equation over $\ell = 1, \dots, m$ for $m \le \mathscr{L}$, multiplying the resulting expression by $\delta t$, and incorporating the assumptions regarding the initial conditions, leads to the conclusion that

$$\max_{m=1,..,\mathscr{L}} \left[\|Q^m\|^2 + \|S^m\|_{,4}^4 + \|S^m\|^2\right] + \sum_{\ell=1}^m \|Q^\ell - Q^{\ell-1}\|^2 + \sum_{\ell=1}^m \|S^\ell - S^{\ell-1}\|^2$$
$$+2\sum_{\ell=1}^m \delta t\|\nabla Q^\ell\|_0^2 + \sum_{\ell=1}^m \delta t\|S^\ell\|_{,4}^4 + 2\sum_{\ell=1}^m \delta t\|S^\ell\|^2$$
$$\le \|Q^0\|^2 + \|S^0\|^2 + \|S^0\|_{,4}^4 + C(\delta t)^3. \tag{58}$$

□

### 5.1 Existence of the approximations

Using a similar methodology as detailed in [18,19,20,21,27,25,28,3,26,5,6,22,23,4], we define the functions $A_s : \Upsilon \times \Upsilon \to \Upsilon$ and $A_q : \Upsilon \times \Upsilon \to \Upsilon$. This formulation is intended to demonstrate the existence of solutions $S$ and $Q$ for the system (48) and (49), for $\ell \geq 1$, where $S^{\ell-1}$ and $Q^{\ell-1}$ are given. This solution satisfies, for all $\eta \in \Upsilon$, that

$$\big(A_q(S,Q),\eta\big) = \big(Q - Q^{\ell-1},\eta\big) + \delta t\big(\nabla Q,\, \nabla\eta\big) + \delta t\big(S^3,\eta\big), \tag{59}$$

$$\big(A_s(S,Q),\eta\big) = \big(S - S^{\ell-1},\eta\big) + \delta t\big(S,\eta\big) - \delta t\big(Q,\eta\big). \tag{60}$$

The continuous piecewise linear functions $A_s$ and $A_q$ are uniquely determined by their values at the nodal points $\mathscr{N}$, as outlined below. This uniqueness is verified by substituting $\eta \equiv \varphi_j$ into equations (59) and (60) for $j = 0,\ldots,J$, resulting in solvable square matrix systems.

$$\widehat{M}A_s(S,Q) = S_1,$$

$$\widehat{M}A_q(S,Q) = S_2.$$

Here, the matrix $\widehat{M}$ represents the lumped mass matrix previously introduced. The vectors $S_1$ and $S_2$ are constructed using the nodal values of $S$, $Q$, $S^{\ell-1}$, and $Q^{\ell-1}$. As a result, the functions $A_s$ and $A_q$ are clearly and uniquely defined.

Equations (59) and (60) allow us to reformulate the problem $(\Psi^{,\delta t})$ in the following manner:
For given $\{S^0, Q^0\} \in \Upsilon \times \Upsilon$, find $\{S,Q\} \in \Upsilon \times \Upsilon$, $\ell \geq 1$, such that

$$A_s(S,Q) = 0, \quad A_q(S,Q) = 0. \tag{61}$$

**Lemma 1.** *For every $\mathscr{R} > 0$, the mappings $A_s : [\Upsilon]^2_{\mathscr{R}} \to \Upsilon$ and $A_q : [\Upsilon]^2_{\mathscr{R}} \to \Upsilon$ are continuous functions, where*

$$[\Upsilon]^2_{\mathscr{R}} = \Big\{ \{\eta_1,\eta_2\} \in \Upsilon \times \Upsilon : |\eta_1|^2 + |\eta_2|^2 \leq \mathscr{R}^2 \Big\}.$$

**Proof**: Given $\{S_1,Q_1\},\{S_2,Q_2\} \in [\Upsilon]^2$, it follows from (59) that for any $\eta \in \Upsilon$, the following relationship is satisfied:

$$\big(A_q(S_1,Q_1) - A_q(S_2,Q_2),\eta\big) = \big(Q_1 - Q_2,\eta\big) + \delta t\big(\nabla Q_1 - \nabla Q_2,\, \nabla\eta\big) + \delta t\big(S_1^3 - S_2^3,\eta\big). \tag{62}$$

Selecting $\eta = A_q(S_1,Q_1) - A_q(S_2,Q_2)$ in (62) and applying the Cauchy-Schwarz inequality alongside (24) and (15), we obtain the following conclusion:

$$\begin{aligned}\big|A_q(S_1,Q_1) - A_q(S_2,Q_2)\big|^2 \leq\; & \big|Q_1 - Q_2\big|\big|A_q(S_1,Q_1) - A_q(S_2,Q_2)\big| \\ &+ Ch^{-1}\delta t\big|Q_1 - Q_2\big|\big|A_q(S_1,Q_1) - A_{sq}(S_2,Q_2)\big| \\ &+ \delta t\big|S_1^3 - S_2^3\big|\big|A_q(S_1,Q_1) - A_q(S_2,Q_2)\big|.\end{aligned} \tag{63}$$

The Cauchy-Schwarz inequality implies that

$$\delta t\big|S_1^3 - S_2^3\big| \leq C\delta t\big(|S_1|^2_{,\infty} + |S_2|^2_{,\infty}\big)\big|S_1 - S_2\big| \;\leq\; C\delta t\big|S_1 - S_2\big|. \tag{64}$$

Using (63) and (64), it follows that

$$\big|A_q(S_1,Q_1) - A_q(S_2,Q_2)\big| \leq C(\delta t, h^{-1})\big(|S_1 - S_2| + |Q_1 - Q_2|\big). \tag{65}$$

From (60), we conclude, for every $\eta \in \Upsilon$, that

$$\big(A_s(S_1,Q_1) - A_s(S_2,Q_2),\, \eta\big) = \big(S_1 - S_2,\eta\big) + \delta t\big(S_1 - S_2,\eta\big) - \delta t\big(Q_1 - Q_2,\eta\big). \tag{66}$$

Setting $\eta = A_s(S_1,Q_1) - A_s(S_2,Q_2)$ and applying the Cauchy-Schwarz inequality, we arrive at the following:

$$\begin{aligned}\big|A_s(S_1,Q_1) - A_s(S_2,Q_2)\big|^2 \leq\; & \big|S_1 - S_2\big|\big|A_s(S_1,Q_1) - A_s(S_2,Q_2)\big| \\ &+ \delta t\big|S_1 - S_2\big|\big|A_s(S_1,Q_1) - A_s(S_2,Q_2)\big| \\ &+ \delta t\big|Q_1 - Q_2\big|\big|A_s(S_1,Q_1) - A_s(S_2,Q_2)\big|.\end{aligned} \tag{67}$$

Therefore, we can infer that

$$\big|A_s(S_1,Q_1) - A_s(S_2,Q_2)\big| \leq C\delta t\big(\big|S_1 - S_2\big| + \big|Q_1 - Q_2\big|\big). \tag{68}$$

The results in (65) and (68) show that $A_s$ and $A_q$ are Lipschitz continuous, respectively. □

**Theorem 3.** *Let $S^{\ell-1}$ and $Q^{\ell-1} \in \Upsilon$ represent the solution at the $(\ell-1)$-th iteration of $(\Psi^{,\delta t})$, where $\ell = 1, 2, \ldots, \mathscr{L}$. Then, for every $> 0$, there exists a solution pair $\{S, Q\} \in [\Upsilon]^2_{\mathscr{R}}$ corresponding to the $\ell$-th iteration of $(\Psi^{,\delta t})$.*

**Proof**: Let $\mathscr{R} > 0$, and suppose that there is no pair $\{S, Q\} \in \Upsilon \times \Upsilon$ such that $A_s(S, Q) = A_q(S, Q) = 0$. Given that the functions $A_s(S, Q)$ and $A_q(S, Q)$ are continuous over $[\Upsilon]^2_{\mathscr{R}}$, we can define a continuous mapping $\mathscr{B} : [\Upsilon]^2_{\mathscr{R}} \to [\Upsilon]^2_{\mathscr{R}}$ as follows:

$$\mathscr{B}(S, Q) = (\mathscr{B}_s(S, Q), \mathscr{B}_q(S, Q)),$$

where $\mathscr{B}_s(S, Q)$ and $\mathscr{B}_q(S, Q)$ are as follows:

$$\begin{aligned} \mathscr{B}_s(S, Q) &:= \frac{-\mathscr{R} A_s(S, Q)}{|(A_s(S, Q), A_q(S, Q))|_{\Upsilon \times \Upsilon}}, \\ \mathscr{B}_q(S, Q) &:= \frac{-\mathscr{R} A_q(S, Q)}{|(A_s(S, Q), A_q(S, Q))|_{\Upsilon \times \Upsilon}}, \end{aligned} \tag{69}$$

where $|(.,.)|_{[\Upsilon]^2_{\mathscr{R}}}$ is the standard norm on $[\Upsilon]^2_{\mathscr{R}}$ defined by

$$|(\chi_1, \chi_2)|_{\Upsilon \times \Upsilon} = (\sum_{i=1}^{2} |\chi_i|^2)^{\frac{1}{2}}.$$

The continuity of the function $\mathscr{B}$ follows directly from the continuity of $A_s$ and $A_q$, as established in Lemma 1. Since $[\Upsilon]^2_{\mathscr{R}}$ is a convex and compact subset of $\Upsilon \times \Upsilon$, Schauder's fixed-point theorem guarantees the existence of $S, Q \in [\Upsilon]^2_{\mathscr{R}}$ that are fixed points of $\mathscr{B}$, expressed as:

$$\mathscr{B}(S, Q) = (\mathscr{B}_s(S, Q), \mathscr{B}_q(S, Q)) = (S, Q).$$

Additionally, from (69), it is evident that the fixed point $\{S, Q\}$ satisfies:

$$|S|^2 + |Q|^2 = |\mathscr{B}_s(S, Q)|^2 + |\mathscr{B}_q(S, Q)|^2 = \mathscr{R}^2. \tag{70}$$

By setting $\eta \equiv Q$ in (59) and $\eta \equiv \pi S^3$ in (60), it follows that:

$$\big(A_q(S, Q), Q\big) = \big(Q - Q^{\ell-1}, Q\big) + \delta t\,(\nabla Q,\, \nabla Q) + \delta t\,(S^3, Q), \tag{71}$$

$$\big(A_s(S, Q), \pi S^3\big) = \big(S - S^{\ell-1}, \pi S^3\big) + \delta t\big(S, \pi S^3\big) - \delta t\big(Q, \pi S^3\big). \tag{72}$$

From (51) and the application of Young's inequality, we deduce that

$$(Q - Q^{\ell-1}, Q) \geq \frac{1}{2}\big(|Q|^2 - |Q^{\ell-1}|^2\big), \tag{73}$$

and

$$(S - S^{\ell-1}, \pi S^3) \geq \frac{1}{2}\big(|S|^4_{,4} - |S^{\ell-1}|^4_{,4}\big). \tag{74}$$

By combining (71) and (72), and taking into account (73) along with Young's inequality, we conclude that for $\mathscr{R}$ sufficiently large:

$$\begin{aligned} \big(A_q(S, Q), Q\big) + \big(A_s(S, Q), S^3\big) &\geq \frac{1}{2}\big|Q\big|^2 - \frac{1}{2}|Q^{\ell-1}|^2 + \frac{1}{2}|S|^4_{,4} - \frac{1}{2}|S^{\ell-1}|^4_{,4} + \delta t|Q|^2_1 + \delta t|S|^4_{,4} \\ &\geq \min\{\delta t\}\big\{\big|Q\big|^2 + \big|S\big|^4_{,4}\big\} - C(Q^{\ell-1}, S^{\ell-1}) \\ &\geq \mathscr{R}^2 - C(Q^{\ell-1}, S^{\ell-1}) \geq 0. \end{aligned} \tag{75}$$

Acknowledging that $\{S, Q\}$ is a fixed point of the function $\mathscr{B}$, and taking into account (69) and (75), we deduce that for sufficiently large $\mathscr{R}$, the following relation holds:

$$(Q,\, Q) + (S, \pi S^3) = \frac{-\mathscr{R}[(A_q(S, Q), S) + (A_s(S, Q), \pi S^3)]}{|(A_s(S, Q), A_q(S, Q))|_{\Upsilon \times \Upsilon}} < 0. \tag{76}$$

From (70), it follows that:

$$(Q, Q) + (S,\ \pi S^3) = |Q|^2 + |S|^4_{,4} = \mathscr{R}^2 \geq 0. \tag{77}$$

It is evident that (77) contradicts (76). This contradiction ensures the existence of a pair $\{S, Q\} \in \Upsilon \times \Upsilon$ such that $A_s(S, Q) = A_q(S, Q) = 0$. Consequently, this implies the existence of a solution, denoted as $\{S, Q\}$, for the $n$-th time step of the problem $(\Phi^{,\delta t})$. □

### 5.2 Existence of a weak solution

We start by presenting the following definitions:

$$S(t) = \Big(\frac{t - t_{\ell-1}}{\delta t}\Big)S^{\ell} + \Big(\frac{t_\ell - t}{\delta t}\Big)S^{\ell-1}, \quad t \in [t_{\ell-1}, t_\ell], \ell \geq 1, \tag{78}$$

$$Q(t) = \Big(\frac{t - t_{\ell-1}}{\delta t}\Big)Q^{\ell} + \Big(\frac{t_\ell - t}{\delta t}\Big)Q^{\ell-1}, \quad t \in [t_{\ell-1}, t_\ell], \ell \geq 1, \tag{79}$$

and

$$S^+(t) = S^\ell, \quad S^-(t) = S^{\ell-1}, \quad t \in (t_{\ell-1}, t_\ell], \ell \geq 1, \tag{80}$$

$$Q^+(t) = Q^\ell, \quad Q^-(t) = Q^{\ell-1}, \quad t \in (t_{\ell-1}, t_\ell], \ell \geq 1. \tag{81}$$

After identifying equations (78), (79), (80), and (81), it can be concluded that

$$\frac{\partial S}{\partial t} = \frac{S^+ - S^-}{\delta t} = \frac{S^+ - S}{t_\ell - t} = \frac{S - S^-}{t - t_{\ell-1}}, \quad t \in (t_{\ell-1}, t_\ell), \ell \geq 1, \tag{82}$$

$$\frac{\partial Q}{\partial t} = \frac{Q^+ - Q^-}{\delta t} = \frac{Q^+ - Q}{t_\ell - t} = \frac{Q - Q^-}{t - t_{\ell-1}}, \quad t \in (t_{\ell-1}, t_\ell), \ell \geq 1. \tag{83}$$

By utilizing the notation introduced earlier for problem $(\Psi^{,\delta t})$, we can express it in the following form:

$$\int_0^{\mathscr{M}} (\frac{\partial Q}{\partial t}, \eta)dt + \int_0^{\mathscr{M}} (\nabla Q^+, \nabla \eta)dt + \int_0^{\mathscr{M}} ((S^+)^3, \eta)dt = 0, \tag{84}$$

$$\int_0^{\mathscr{M}} (\frac{\partial S}{\partial t}, \eta)dt + \int_0^{\mathscr{M}} (S^+, \eta)dt - \int_0^{\mathscr{M}} (Q^+, \eta)dt = 0. \tag{85}$$

**Theorem 4.** *Assuming the conditions of Theorem (2) hold, there exists a subsequence of $\{S^\pm, Q^\pm\}$ that solves (84) and (85) as $h \to 0$, such that:*

$$S, S^\pm \rightharpoonup^* s \quad \text{in} \quad L^\infty(0, \mathscr{M}; L^4(\Psi)), \tag{86}$$

$$Q, Q^\pm \rightharpoonup^* q \quad \text{in} \quad L^\infty(0, \mathscr{M}; L^2(\Psi)), \tag{87}$$

$$S, S^\pm \rightharpoonup^* s \quad \text{in} \quad L^\infty(0, \mathscr{M}; L^2(\Psi)), \tag{88}$$

$$Q, Q^\pm \rightharpoonup q \quad \text{in} \quad L^2(0, \mathscr{M}; H^1(\Psi)), \tag{89}$$

$$S, S^\pm \to s \quad \text{in} \quad L^4(\Psi_{\mathscr{M}}), \tag{90}$$

$$Q, Q^\pm \to q \quad \text{in} \quad L^2(\Psi_{\mathscr{M}}), \tag{91}$$

$$\partial_t Q \rightharpoonup \partial_t q \quad \text{in} \quad L^{\frac{3}{4}}(0, \mathscr{M}; (H^1(\Psi))'), \tag{92}$$

$$\partial_t S \rightharpoonup \partial_t s \quad \text{in} \quad L^2(0, \mathscr{M}; (L^2(\Psi))'). \tag{93}$$

**Proof**: The convergence results above are derived from the bounds in (2) and the fact that the spaces $L^2(0, \mathscr{M}; (L^2(\Psi))')$, $L^2(0, \mathscr{M}; (H^1(\Psi))')$, and $L^4(\Psi_{\mathscr{M}})$ are reflexive Banach spaces. Furthermore, the spaces $L^2(0, \mathscr{M}; H^1(\Psi))$, $L^\infty(0, \mathscr{M}; L^4(\Psi))$, and $L^\infty(0, \mathscr{M}; L^2(\Psi))$ are the duals of $L^1(0, \mathscr{M}; (H^1(\Psi))')$, $L^1(0, \mathscr{M}; L^{4/3}(\Psi))$, and $L^1(0, \mathscr{M}; L^2(\Psi))$, respectively. While these dual spaces are separable Banach spaces, they are not reflexive. □

## 6 Computational results

In order to verify the theoretical results and illustrate the practicality of the approximated solutions, this section presents computations in both one and two dimensions. First, an efficient algorithm was developed to compute the approximated solutions. Next, the computations were executed in both one- and two-dimensional spaces. Additionally, the results for the fully-discrete system in one and two dimensions were analyzed and presented. All computations were performed using a fully numerical approach. All computations in this study were done with a fully numerical finite element implementation. We used piecewise linear basis functions for spatial discretization, and we applied an implicit backward Euler method for time integration. We solved the resulting nonlinear systems at each time step with a Gauss-Seidel method. All matrix assembly, linear algebra operations, and post-processing were done numerically in MATLAB (R2023a) without symbolic computation. This numerical approach guarantees efficiency, scalability to higher dimensions, and the ability to reproduce results.

## 6.1 Computational algorithm

To address the nonlinear algebraic system arising from the approximated problem, denoted as $(\Phi^{,\delta t})$, at each time step, we introduce the following efficient solution formula:
$(\Phi_{\iota}^{,\delta t})$: Given $Q^{\ell,0}, S^{\ell,0} \in \Upsilon$, then for $\iota \geq 1$ find $\{Q^{\ell,\iota}, S^{\ell,\iota}\} \in \Upsilon \times \Upsilon$, for all $\eta \in \Upsilon$, such that

$$\Big(\frac{Q^{\ell,\iota} - Q^{\ell-1}}{\delta t}, \eta\Big) + (\nabla Q^{\ell,\iota}, \nabla\eta) + ((S^{\ell,\iota})^3, \eta) = 0, \tag{94}$$

$$\Big(\frac{S^{\ell,\iota} - S^{\ell-1}}{\delta t}, \eta\Big) + (S^{\ell,\iota}, \eta) - (Q^{\ell,\iota}, \eta) = 0. \tag{95}$$

The process begins with the definitions $Q^0 \equiv \pi^{q0}$ and $S^0 \equiv \pi^{s0}$. For time steps $\ell \geq 1$, we initialize $Q^{\ell,0}$ as $Q^{\ell-1}$ and $S^{\ell,0}$ as $S^{\ell-1}$. To formulate a linear system of equations, the system (94) and (95) is tested against $\varphi_j$, where $j$ ranges from 0 to $J$. This results in $2 \times (J+1)^d$ linear equations. The Gauss-Seidel iteration method is employed to solve this system. Although the convergence of the Gauss-Seidel method has not been formally established, numerical experiments at each time step demonstrate that it converges within only a few iterations. To ensure the accuracy of the iterative solution, the following stopping criteria are employed:

$$\max\left\{|Q^{\ell,\iota} - Q^{\ell,\iota-1}|_{0,\infty}, |S^{\ell,\iota} - S^{\ell,\iota-1}|_{0,\infty}\right\} < \rho = 10^{-8}. \tag{96}$$

If the condition stated earlier is met, we update the values as follows: $S^{\ell} \equiv S^{\ell,\iota}$ and $Q^{\ell} \equiv Q^{\ell,\iota}$.

## 6.2 Error computations

To evaluate the error, we modify the problem $(\Phi)$ by adding a source term $f(\mathbf{x},t)$ and $g(\mathbf{x},t)$. This modification changes the system represented by equations (4) and (5) into the following form:

$$\partial_t q - \Delta q + s^3 = f(\mathbf{x},t), \tag{97}$$

$$\partial_t s + s - q = g(\mathbf{x},t). \tag{98}$$

As a result, we examine the following improved FE approximation of problem $(\Phi_{\iota}^{,\delta t})$:
$(\Phi_{\iota}^{,\delta t})$: Given $Q^{\ell,0}, S^{\ell,0} \in \Upsilon$, find $\{Q^{\ell,\iota}, S^{\ell,\iota}\} \in \Upsilon \times \Upsilon$, for all $\eta \in \Upsilon$, such that

$$\Big(\frac{Q^{\ell,\iota} - Q^{\ell-1}}{\delta t}, \eta\Big) + (\nabla Q^{\ell,\iota}, \nabla\eta) + ((S^{\ell,\iota})^3, \eta) = (f(\mathbf{x},t), \eta), \tag{99}$$

$$\Big(\frac{S^{\ell,\iota} - S^{\ell-1}}{\delta t}, \eta\Big) + (S^{\ell,\iota}, \eta) - (Q^{\ell,\iota}, \eta) = (g(\mathbf{x},t), \eta). \tag{100}$$

### 6.2.1 One-dimensional error

This section provides two computational examples to solve the system defined by equations (99) and (100) under homogeneous Dirichlet boundary conditions and predefined initial conditions. To simplify the analysis, all examples are conducted within the spatial domain $\Psi = [0,1]$ and over a time interval $\mathscr{M} = 1$. The initial conditions, boundary conditions, and source terms $f(x,t)$ and $g(x,t)$ are tailored to align with the exact solution for each case. The spatial domain $\Psi = [0,1]$ is initially divided uniformly into $J$ intervals, forming a square mesh. Each element of the mesh has a size denoted by $h = 1/J$, while the time step is chosen as $\delta t = 10^{-4}$. The exact solutions are defined as follows:

$$s(x,t) = \sin(2\pi x)\exp(-2t).$$

The errors in the $L^1$, $L^2$, and $L^\infty$ norms are provided in Table 1.

### 6.2.2 Two-dimensional error

In a two-dimensional context, governed by the system described in equations (99) and (100) with Dirichlet boundary and initial conditions, the spatial domain is confined to $\Psi = [0,1] \times [0,1]$. For simplicity, the time interval is defined as $[0, \mathscr{M}] = [0,1]$. The initial and boundary conditions, as well as the source terms $f(x,y,t)$ and $g(x,y,t)$, are specified to correspond to the exact solution for each case. A time step of $\delta t = 10^{-4}$ is used for the simulations. The exact solution is given by:

$$s(x,y,t) = \sin(2\pi x)\sin(2\pi y)\exp(-2t).$$

The errors in the $L^1$, $L^2$, and $L^\infty$-norms for these simulations are presented in Table 2.

| $J$ | $L^1$ | $L^2$ | $L^\infty$ |
|---|---|---|---|
| 10 | 3.27E-03 | 1.19E-03 | 4.55E-03 |
| 20 | 7.82E-04 | 1.96E-04 | 1.18E-03 |
| 25 | 4.98E-04 | 1.11E-04 | 7.50E-04 |
| 40 | 1.91E-04 | 3.36E-05 | 2.93E-04 |
| 100 | 1.22E-04 | 1.91E-05 | 1.87E-04 |
| 200 | 3.01E-05 | 3.34E-06 | 4.68E-05 |
| 250 | 7.49E-06 | 5.88E-07 | 1.17E-05 |
| 400 | 4.79E-06 | 3.37E-07 | 7.50E-06 |

**Table 1:** Discrete $L^1, L^2, L^\infty$-norms error for one-dimensional example.

| $J$ | $L^1$ | $L^2$ | $L^\infty$ |
|---|---|---|---|
| 10 | 2.18E-03 | 2.88E-04 | 4.22E-03 |
| 20 | 5.07E-04 | 3.18E-05 | 1.15E-03 |
| 25 | 3.21E-04 | 1.59E-05 | 7.30E-04 |
| 40 | 1.21E-04 | 3.76E-06 | 2.86E-04 |
| 100 | 7.69E-05 | 1.90E-06 | 1.82E-04 |

**Table 2:** Discrete $L^1, L^2, L^\infty$-norms error for two-dimensional example.

| $J$ | $L^1$ | $L^2$ | $L^\infty$ |
|---|---|---|---|
| 10 | 2.89E-02 | 1.38E-03 | 7.76E-02 |
| 20 | 2.68E-02 | 4.21E-04 | 9.13E-02 |
| 25 | 2.66E-02 | 2.92E-04 | 9.09E-02 |
| 40 | 2.53E-02 | 1.38E-04 | 9.16E-02 |
| 100 | 2.50E-02 | 9.74E-05 | 9.11E-02 |

**Table 3:** Discrete $L^1, L^2, L^\infty$-norms error for three-dimensional example.

### 6.2.3 Three-dimensional error

In this section, we provide a three-dimensional example, focusing on the system described by (99) and (100) with Dirichlet boundary and initial conditions. For this case, the spatial domain is simplified to $\Psi = [0,1] \times [0,1] \times [0,1]$, and the time interval is set as $[0,\mathscr{M}] = [0,1]$. The initial and boundary conditions, together with the source terms $f(x,y,z,t)$ and $g(x,y,z,t)$, are defined to align with the exact solution specific to each scenario. A time step of $\delta t = 10^{-4}$ is used. The exact solution is specified as follows:

$$s(x,y,z,t) = \sin(2\pi x)\sin(2\pi y)\sin(2\pi z)\exp(-2t).$$

The errors in the $L^1$, $L^2$, and $L^\infty$-norms for these simulations are shown in Table 3.

Tables 1, 2, and 3 show the discrete $L^1$, $L^2$, and $L^\infty$ norm errors of the proposed numerical method for the one-, two-, and three-dimensional versions of the strongly damped nonlinear wave equation. As the mesh size, or grid resolution $J$, increases, we see a consistent reduction in error across all norms. This confirms that the method is both stable and convergent.

In the two-dimensional example (Table 2), the $L^1$, $L^2$, and $L^\infty$ norm errors drop sharply as $J$ grows from 10 to 100. This shows second-order accuracy in space. Such behavior suggests that the numerical discretization captures the spatial changes in the solution well, without causing much numerical diffusion or dispersion.

For the three-dimensional example (Table 3), the initial errors are slightly larger due to increased complexity, but the scheme still shows a steady decline in error with improved grid resolution. Notably, the $L^2$ norm displays almost a steady decrease, demonstrating the method's strength in multi-dimensional cases. The slight changes in the $L^\infty$ norm are expected because of nonlinear interactions and boundary effects in higher dimensions. Overall, the numerical results confirm that the proposed method yields accurate, stable, and converging approximations for the strongly damped nonlinear wave equation across different spatial dimensions.

## *6.3 Two-dimensional simulations*

*Example 1.*We choose the initial data as [7]:

$$s(x,y,0) = \exp(-(x+2)^2 - y^2) + \exp(-(x-2)^2 - y^2), \ x,y \in [-8,8] \times [-8,8], \tag{101}$$

$$s_t(x,y,0) = \exp(-x^2 - y^2), \qquad x,y \in [-8,8] \times [-8,8]. \tag{102}$$

We solve this model with the following parameter values: $\delta t = 0.000001$, and $J = 320$. The solutions of this example at $\mathscr{M} = 0, 0.3, 1, 2, 4$ and 5.5 are shown in Figure 1. Figure 1 displays the time evolution of the numerical solution $s(x,y)$ for Example 1 governed by the strongly damped nonlinear wave equation. The initial condition consists of two symmetric Gaussian humps centered at $x = \pm 2$ (see Eqs. (101)–(102)), which interact and evolve over time. As the time variable $\mathscr{M}$ increases from 0 to 5.5, the two distinct peaks gradually merge due to the combined effects of strong damping and nonlinear diffusion. The early stages of humps' separation and interaction are depicted in subfigures (a)–(c), whereas the later stages of energy dissipation and the appearance of a single smooth structure close to the origin are shown in subfigures (d)–(f). This numerical behavior demonstrates how the strong damping term $-\Delta s_t$ stabilizes the solution by effectively suppressing oscillations and guiding it toward a steady state.

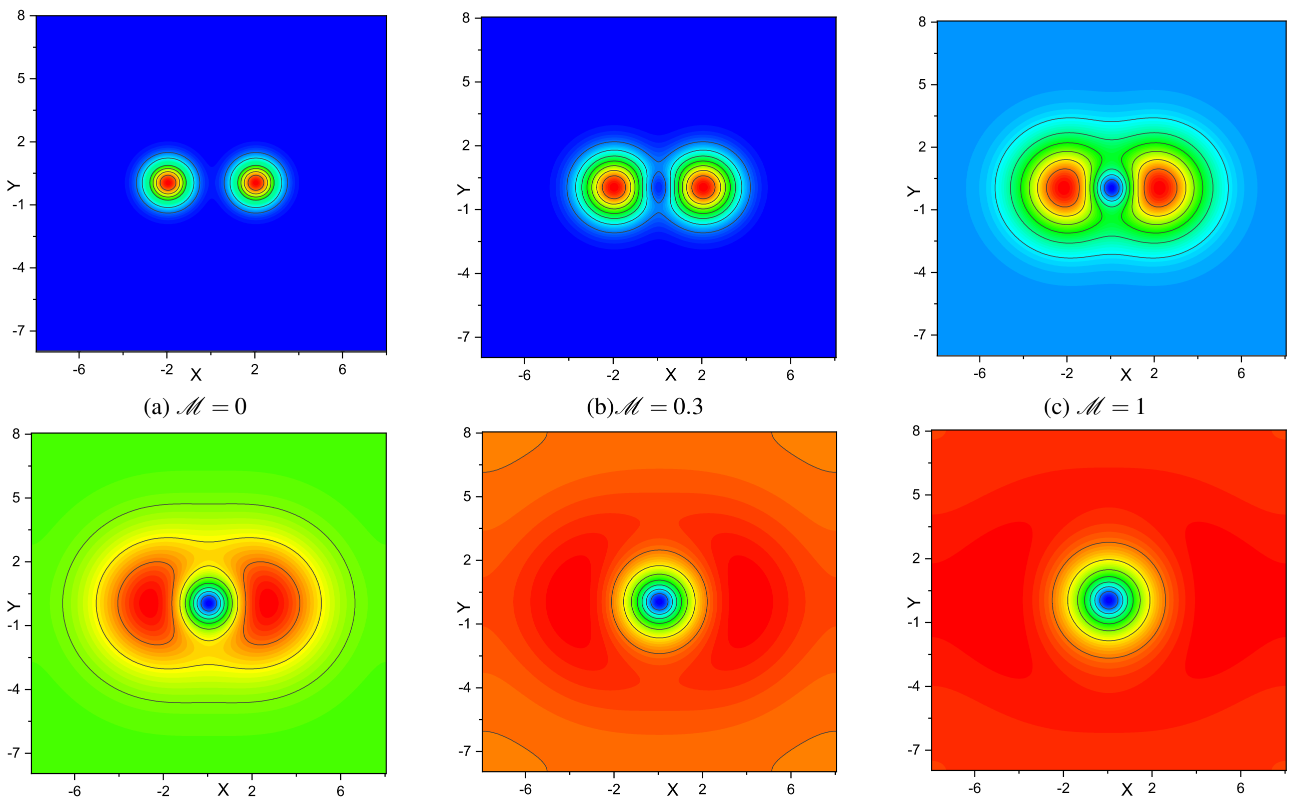


(a) $\mathscr{M} = 0$ (b).$\mathscr{M} = 0.3$ (c) $\mathscr{M} = 1$

(d) $\mathscr{M} = 2$ (e) $\mathscr{M} = 4$ (f) $\mathscr{M} = 5.5$

**Fig. 1:** The solution $s(x,y)$ for Example 1

*Example 2.*In this example the following initial conditions has been considered [54]:

$$s(x,y,0) = \begin{cases} -(x^{\frac{2}{3}} + y^{\frac{2}{3}} + 0.1) & \text{if } x^{\frac{2}{3}} + y^{\frac{2}{3}} \le 0.7^{\frac{2}{3}}, \quad x,y \in [-1,1] \times [-1,1], \\ 0 & \text{otherwise} , \end{cases} \tag{103}$$

$$s_t(x,y,0) = 10s(x,y,0), \qquad x,y \in [-1,1] \times [-1,1]. \tag{104}$$

This example is solved at $\delta t = 0.000001$. The answers to this example at $\mathscr{M} = 0, 0.3, 0.6$, and 1 are provided in Figure 2. The temporal evolution of the numerical solution $s(x,y)$ for Example 2 is shown in Figure 2. This solution is initialized with a non-smooth, diamond-shaped profile defined by Eqs. (103)–(104). The piecewise definition of the initial condition is characterized by sharp corners and steep gradients, which are present in the solution at the initial time $\mathscr{M} = 0$. Panels (b)–(d) show how the strong damping term $-\Delta s_t$ in the governing equation introduces diffusion and smoothing effects as time passes. With energy dissipating over time, the initially sharp structure quickly transforms into a smooth, symmetric profile centered at the origin. This change demonstrates the damping mechanism's potent regularizing power, which guarantees the decay of high-frequency components and stabilizes the numerical solution, guiding the system toward a stable, spatially smooth configuration.

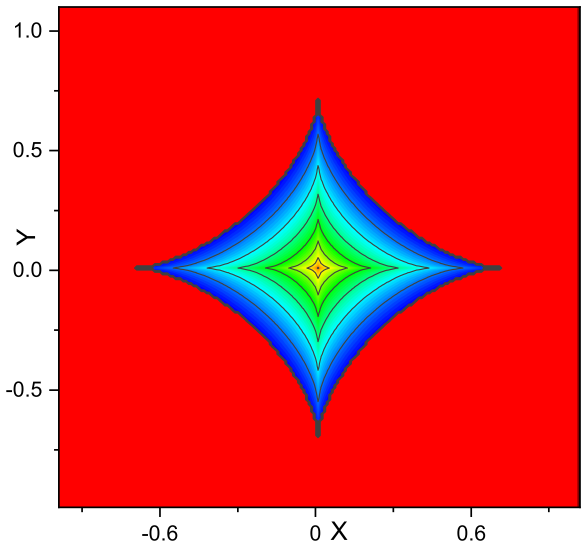


(a) $\mathscr{M} = 0$

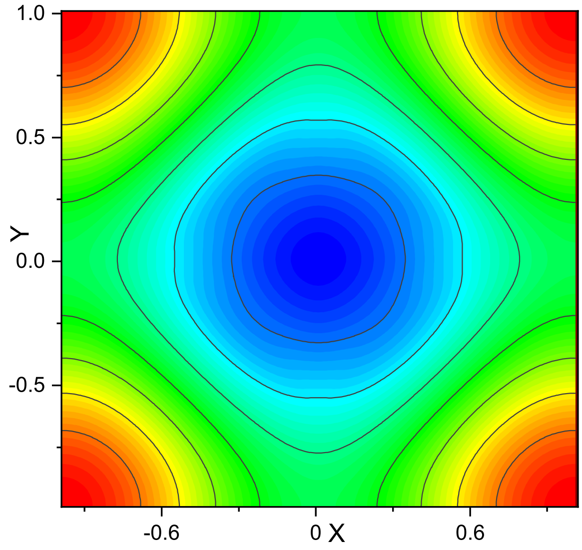


(b).$\mathscr{M} = 0.3$

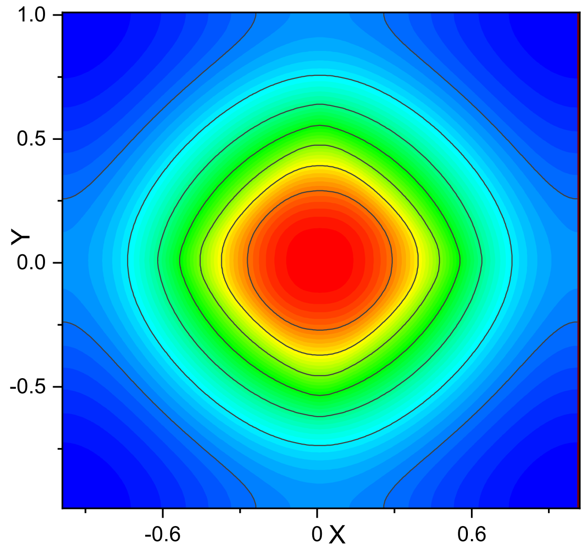


(c) $\mathscr{M} = 0.6$

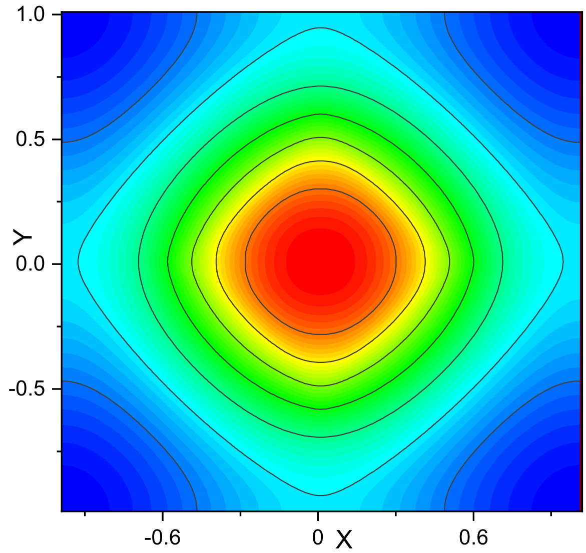


(d) $\mathscr{M} = 1$

**Fig. 2:** The solution $s(x,y)$ for Example 2

## 7 Conclusions

FE analysis of strongly damped wave equations has been studied in this paper. The order of the differential equation with respect to the time derivative has been transformed from second order to first order. Then, Galerkin FEM has been applied to strongly damped wave equations with stability guarantees under general FE spaces and this method providing accurate solutions for this equation. Moreover, this method is effective for strongly damped wave equations with rapidly varying data and provides improved numerical stability. The approach used in this article can also adapt to stochastic versions of these equations, with error estimates provided for semilinear stochastic models.

## Declarations

**Competing interests**: We declare no competing interests.
**Authors' contributions**: M. H. Hashim completed the theoretical work of the article. S. M. Hassan completed the numerical results. A. J. Harfash proposed the problem and wrote the article.
**Funding**: This article has not received any financial support.
**Availability of data and materials**: The information backing the findings of this study is included in the article.
**Acknowledgments**:The authors express their sincere gratitude to both reviewers for their perceptive remarks and practical recommendations. Their helpful criticism has greatly improved the work's quality and clarity.

## References

[1] T. Achouri. Finite difference schemes for the two-dimensional semilinear wave equation. *Numerical Methods for Partial Differential Equations*, 35(1):200–221, 2019.
[2] S. Ahmed, S. Jahan, and K. Nisar. Haar wavelet collocation method for telegraph equations with different boundary conditions. *Jordan Journal of Mathematics and Statistics*, 17(1):1–21, 2024.
[3] G. A. Al-Juaifri and A. J. Harfash. Finite element analysis of nonlinear reaction–diffusion system of Fitzhugh–Nagumo type with Robin boundary conditions. *Mathematics and Computers in Simulation*, 203:486–517, 2023.
[4] G. A. Al-Juaifri and A. J. Harfash. Numerical analysis of the Brusselator model with robin boundary conditions. *SeMA Journal*, 82:351397, 2024.
[5] G. A. Al-Musawi and A. J. Harfash. Finite element analysis of extended Fisher-Kolmogorov equation with Neumann boundary conditions. *Applied Numerical Mathematics*, 201:41–71, 2024.
[6] G. A. Al-Musawi and A. J. Harfash. Finite element approximation of coupled Cahn-Hilliard equations with a logarithmic potential and nondegenerate mobility. *Journal of Mathematical Modeling*, 13(1):49–68, 2025.
[7] W. Bao and X. Zhao. Comparison of numerical methods for the nonlinear Klein-Gordon equation in the nonrelativistic limit regime. *Journal of Computational Physics*, 398:108886, 2019.
[8] J. W. Barrett and J. F. Blowey. An error bound for the finite element approximation of the Cahn-Hilliard equation with logarithmic free energy. *Numerische Mathematik*, 72(1):1–20, 1995.
[9] T. Cazenave. *Semilinear Schrodinger Equations*, volume 10. Courant Lecture Notes in Mathematics, New York University, Courant Institute of Mathematical Sciences, New York, 2003.
[10] P. G. Ciarlet. *The Finite Element Method for Elliptic Problems*. SIAM, 2002.
[11] P. G. Ciarlet and P.-A. Raviart. General lagrange and hermite interpolation in $R^n$ with applications to finite element methods. *Archive for Rational Mechanics and Analysis*, 46(3):177–199, 1972.
[12] J. Ciavaldini. Analyse numerique dun problème de stefan à deux phases par une methode déléments finis. *SIAM Journal on Numerical Analysis*, 12(3):464–487, 1975.
[13] F. Colombo. An inverse problem for the strongly damped wave equation with memory. *Nonlinearity*, 20(3):659, 2007.
[14] A. del Pilar Márquez and M. de los Santos Bruzón. Conservation laws and symmetry analysis for a quasi-linear strongly-damped wave equation. *Journal of Mathematical Chemistry*, 58(7):1489–1498, 2020.
[15] G. Duvaut. *Lions, Inequalities in Mechanics and Physics*. Berlin–Heidelberg–New York: Springer, 1976.
[16] P. J. Graber and J. L. Shomberg. Attractors for strongly damped wave equations with nonlinear hyperbolic dynamic boundary conditions. *Nonlinearity*, 29(4):1171, 2016.
[17] M. J. Grote and T. Mitkova. High-order explicit local time-stepping methods for damped wave equations. *Journal of Computational and Applied Mathematics*, 239:270–289, 2013.
[18] M. H. Hashim and A. J. Harfash. Finite element analysis of a Keller–Segel model with additional cross-diffusion and logistic source. part I: Space convergence. *Computers and Mathematics with Applications*, 89(1):44–56, 2021.
[19] M. H. Hashim and A. J. Harfash. Finite element analysis of a Keller-Segel model with additional cross-diffusion and logistic source. part II: Time convergence and numerical simulation. *Computers and Mathematics with Applications*, 109(1):216–234, 2022.

[20] M. H. Hashim and A. J. Harfash. Finite element analysis of attraction-repulsion chemotaxis system. Part I: Space convergence. *Communications on Applied Mathematics and Computation*, 4(3):1011–1056, 2022.

[21] M. H. Hashim and A. J. Harfash. Finite element analysis of attraction-repulsion chemotaxis system. Part II: Time convergence, error analysis and numerical results. *Communications on Applied Mathematics and Computation*, 4(3):1057–1104, 2022.

[22] M. H. Hashim and A. J. Harfash. Finite element analysis for microscale heat equation with Neumann boundary conditions. *Iranian Journal of Numerical Analysis and Optimization*, 14(3):796–832, 2024.

[23] M. H. Hashim and A. J. Harfash. The convergence of the finite element approximation to the weak solution of attraction-repulsion chemotaxis system with additional self-diffusion term. *Journal of Mathematical Sciences*, 289(2):273–322, 2025.

[24] M. H. Hashim, S. M. Hassan, A. A. Hameed, and A. J. Harfash. Numerical approximations for damped wave equation with neumann boundary conditions. *Mathematics and Computational Sciences*, 6(1):1–18, 2025.

[25] S. M. Hassan and A. J. Harfash. Finite element analysis of a two-species chemotaxis system with two chemicals. *Applied Numerical Mathematics*, 182:148–175, 2022.

[26] S. M. Hassan and A. J. Harfash. Finite element analysis of the two-competing-species Keller–Segel chemotaxis model. *Computational Mathematics and Modeling*, 33(4):443–471, 2022.

[27] S. M. Hassan and A. J. Harfash. Finite element approximation of a Keller–Segel model with additional self-and cross-diffusion terms and a logistic source. *Communications in Nonlinear Science and Numerical Simulation*, 104:106063, 2022.

[28] S. M. Hassan and A. J. Harfash. Finite element analysis of chemotaxis-growth model with indirect attractant production and logistic source. *International Journal of Computer Mathematics*, 100(4):745–774, 2023.

[29] M. Irfan and F. A. Shah. Numerical solution of bioheat transfer model using generalized wavelet collocation method. *Jordan Journal of Mathematics and Statistics*, 15(2):211–229, 2022.

[30] T. Kadri, M. Rahmeni, and K. Omrani. Efficient and accurate numerical methods for nonlinear strongly damped wave equation in 2+ 1 dimensions. *Computers & Mathematics with Applications*, 160:148–160, 2024.

[31] I. Kinnmark. *The shallow water wave equations: formulation, analysis and application*, volume 15. Springer Science & Business Media, 2012.

[32] S. Labidi and K. Omrani. A new conservative fourth-order accurate difference scheme for the nonlinear schrödinger equation with wave operator. *Applied Numerical Mathematics*, 173:1–12, 2022.

[33] S. Larsson, V. Thomée, and L. B. Wahlbin. Finite-element methods for a strongly damped wave equation. *IMA journal of numerical analysis*, 11(1):115–142, 1991.

[34] P. Ljung, A. Målqvist, and A. Persson. A generalized finite element method for the strongly damped wave equation with rapidly varying data. *ESAIM: Mathematical Modelling and Numerical Analysis*, 55(4):1375–1404, 2021.

[35] A. O. McCartney and V. M. Job. Existence and uniqueness of weak solutions and error analysis of the galerkin finite element method for time-dependent convective nanofluid poiseuille flow problems. *Jordan Journal of Mathematics and Statistics*, 17(3):413–428, 2024.

[36] R. E. Mickens and P. Jordan. A positivity-preserving nonstandard finite difference scheme for the damped wave equation. *Numerical Methods for Partial Differential Equations: An International Journal*, 20(5):639–649, 2004.

[37] R. D. Milne. *Applied Functional Analysis: An Introductory Treatment*. Pitman Publishing, 1980.

[38] H. Moghaderi and M. Dehghan. A multigrid compact finite difference method for solving the one-dimensional nonlinear sine-Gordon equation. *Mathematical Methods in the Applied Sciences*, 38(17):3901–3922, 2015.

[39] A. Mohebbi, M. Abbaszadeh, and M. Dehghan. High-order difference scheme for the solution of linear time fractional Klein–Gordon equations. *Numerical Methods for Partial Differential Equations*, 30(4):1234–1253, 2014.

[40] R. Nochetto. Finite element methods for parabolic free boundary problems. *Advances in numerical analysis*, pages 34–95, 1991.

[41] Ö. Oruç. A new numerical treatment based on lucas polynomials for 1d and 2d sinh-Gordon equation. *Communications in Nonlinear Science and Numerical Simulation*, 57:14–25, 2018.

[42] Ö. Oruç. Numerical simulation of two-dimensional and three-dimensional generalized Klein–Gordon–zakharov equations with power law nonlinearity via a meshless collocation method based on barycentric rational interpolation. *Numerical Methods for Partial Differential Equations*, 38(4):1068–1089, 2022.

[43] A. K. Pani and J. Y. Yuan. Mixed finite element method for a strongly damped wave equation. *Numerical Methods for Partial Differential Equations: An International Journal*, 17(2):105–119, 2001.

[44] V. Pata and S. Zelik. Smooth attractors for strongly damped wave equations. *Nonlinearity*, 19(7):1495, 2006.

[45] P.-A. Raviart. The use of numerical integration in finite element methods for solving parabolic equations. *Topics in numerical analysis*, pages 233–264, 1973.

[46] M. Rincon and M. Copetti. Numerical analysis for a locally damped wave equation. *Journal of Applied Analysis & Computation*, 3(2):169–182, 2013.

[47] M. A. Shubov, C. F. Martin, J. P. Dauer, and B. P. Belinskiy. Exact controllability of the damped wave equation. *SIAM journal on control and optimization*, 35(5):1773–1789, 1997.

[48] R. K. Sinha, A. K. Pani, and S. K. Chung. The effect of spatial quadrature on the semidiscrete finite element galerkin method for a strongly damped wave equation. *Numerical Functional Analysis and Optimization*, 24(3-4):311–325, 2003.

[49] R. Temam. *Infinite-Dimensional Dynamical Systems in Mechanics and Physics*, volume 68. Springer Science & Business Media, 2012.

[50] V. Thomée. *Galerkin Finite Element Methods for Parabolic Problems*, volume 1054. Springer, 1984.

[51] V. Thomée and L. Wahlbin. Maximum-norm estimates for finite-element methods for a strongly damped wave equation. *BIT Numerical Mathematics*, 44:165–179, 2004.

[52] N. K. Wadhawan. Numerical approximation of lambert w function for real values by unique method of quadratic approximation. *Jordan Journal of Mathematics and Statistics*, 18(2):285–315, 2025.

[53] Y. Ye. Global existence and blow-up of solutions for higher-order viscoelastic wave equation with a nonlinear source term. *Nonlinear Analysis: Theory, Methods & Applications*, 112:129–146, 2015.

[54] Y.-L. Zhao and X.-M. Gu. A low-rank algorithm for strongly damped wave equations with visco-elastic damping and mass terms. *arXiv preprint arXiv:2308.08888*, 2023.